Sculpturing of photonic crystals by ion beam lithography: towards complete photonic bandgap at visible wavelengths

Saulius Juodkazis,[1,*] Lorenzo Rosa,[1] Sven Bauerdick,[2] Lloyd Peto,[2] Ramy El-Ganainy,[3] and Sajeev John[3,4]

[1]*Centre for Micro-Photonics, Faculty of Engineering and Industrial Sciences Swinburne University of Technology, Hawthorn, VIC, 3122, Australia*
[2]*Raith GmbH, Konrad-Adenauer-Allee, 8 - PHOENIX West 44263 Dortmund, Germany*
[3]*Department of Physics, University of Toronto, Toronto, Ontario M5S 1A7, Canada*
[4]*John@physics.utoronto.ca*
[*]*SJuodkazis@swin.edu.au*

Abstract: Three dimensional (3D) ion beam lithography (IBL) is used to directly pattern 3D photonic crystal (PhC) structures in crystalline titania. The process is maskless and direct write. The slanted pore 3D structures with pore diameters of 100 nm having aspect ratio of 8 were formed. It is shown that chemical enhancement of titania removal up to 5.2 times is possible in XeF_2 gas for the closest nozzle-to-sample distance; the enhancement was ~ 1.5 times for the actual 3D patterning due to a sample tilt. Tolerances of structural parameters and optimization of IBL processing required for the fabrication of PhCs with full photonic bandgap in visible spectral range in rutile are outlined. Application potential of 3D-IBL is discussed.

OCIS codes: (240.6695) Photonic crystals; (350.3850) Materials processing; (160.1245) Artificially engineered materials; (160.4236) Nanomaterials.

References and links

1. S. John, "Strong localization of photons in certain disordered dielectric superlattices," Phys. Rev. Lett. **58**, 2486–2489 (1987).
2. E. Yablonovitch, "Inhibited spontaneous emission in solid-state physics and electronics," Phys. Rev. Lett. **58**, 2059–2062 (1987).
3. S. John, "Loalization of light: theory of photonic band gap materials," in *Photonic band gap materials*, C. Sokoulis, ed. (Kluwer, The Netherlands, 1996).
4. J. D. Joannopoulos, P. R. Villeneuve, and S. Fan, "Photonic crystals: Putting a new twist on light," Nature **386**, 143–149 (1997).
5. S. Johnson and J. D. Joannopoulos, *Photonic crystals: The Road From Theory to Practice* (Kluwer, Dordrecht, The Netherlands, 2002).
6. T. F. Krauss and R. M. de La Rue, "Photonic crystals in the optical regime - past, present and future," Prog. Quantum Electron. **23**, 51–96 (1999).
7. S. Kitson, W. Barnes, and J. Sambles, "Full Photonic Band Gap for Surface Modes in the Visible," Phys. Rev. Lett. **77**, 2670–2673 (1996).
8. A. Blanco, E. Chomski, S. Grabtchak, M. Ibisate, S. John, S. Leonard, C. Lopez, F. Meseguer, H. Miguez, J. Mondia, G. Ozin, O. Toader, and H. van Driel, "Large-scale synthesis of a silicon photonic crystal with a complete three-dimensional bandgap near 1.5 micrometres," Nature **405**, 437–40 (2000).
9. E. Yablonovitch, "Photonic band-gap structures," J. Opt. Soc. Am. **10**, 283–295 (1993).
10. A. Tandaechanurat, S. Ishida, D. Guimard, M. Nomura, S. Iwamoto, and Y. Arakawa, "Lasing oscillation in a three-dimensional photonic crystal nanocavity with a complete bandgap," Nat. Photon. **5**, 91-94 (2011).

#141022 - $15.00 USD Received 12 Jan 2011; revised 1 Mar 2011; accepted 4 Mar 2011; published 14 Mar 2011

11. N. Tétreault, G. von Freymann, M. Deubel, M. Hermatschweiler, F. Pérez-Willard, S. John, M. Wegener, and G. Ozin, "New route to three-dimensional photonic bandgap materials: silicon double inversion of polymer templates," Adv. Mater. **18**, 457–460 (2005).
12. K. K. Seet, V. Mizeikis, K. Kannari, S. Juodkazis, H. Misawa, N. Tetreault, and S. John, "Templating and replication of spiral photonic crystals for silicon photonics," IEEE J. Selec. Topics Quant Electr. **14**, 1064 – 1073 (2008).
13. F. B. McCormick, J. G. Fleming, S. Mani, M. R. Tuck, J. D. Williams, C. L. Arrington, S. H. Kravitz, C. Schmidt, G. Subramania, J. C. Verley, A. R. Ellis, I. El-kady, D. W. Peters, M. W. W. C. Sweatt, and J. J. Hudgens, "Fabrication and characterization of large-area 3-D photonic crystals," in IEEE Aerospace Conf. Proc., 1820–1827 (2006).
14. J. Schilling and A. Scherer, "3D photonic crystals based on macroporous silicon: Towards a large complete photonic bandgap," Photon. Nanostr.: Fund. and Appl. **3**, 90–95 (2005).
15. G. Subramania, Y.-J. Lee, A. J. Fischer, and D. D. Koleske, "Log-pile TiO_2 photonic crystal for light control at near-UV and visible wavelengths," Adv. Mater. **22**, 487–491 (2010).
16. S. Juodkazis, V. Mizeikis, K. K. Seet, H. Misawa, and U. G. K. Wegst, "Mechanical properties and tuning of three-dimensional polymeric photonic crystals," Appl. Phys. Lett. **91**, 241904 (2007).
17. T. Kondo, S. Juodkazis, and H. Misawa, "Reduction of capillary force for high-aspect ratio nanofabrication," Appl. Phys. A **81**, 1583 – 1586 (2005).
18. S. Juodkazis, V. Mizeikis, K. K. Seet, M. Miwa, and H. Misawa, "Two-photon lithography of nanorods in SU-8 photoresist," Nanotechnol. **16**, 846 – 849 (2005).
19. O. Toader and S. John, "Slanted-pore photonic band-gap materials," Phys. Rev. E **71**, 036605 (2005).
20. J. Winkler, *Titanium dioxide* (Vincentz Network, Hannover, 2003).
21. E. D. Palik, ed., *Handbook of Optical Constants of Solids* (Academic Press, New York, 1985).
22. T. Dai, X. Kang, B. Zhang, J. Xu, K. Bao, C. Xiong, and Z. H. Gan, "Study and formation of 2D microstructures of sapphire by focused ion beam milling," Microelectr. Eng. **85**, 640–645 (2008).
23. S. Takahashi, K. Suzuki, M. Okano, M. Imada, T. Nakamori, Y. Ota, K. Ishizaki, and S. Noda, "Direct creation of three-dimensional photonic crystals by a top-down approach," Nat. Mater. **8**, 721–725 (2009).
24. L. Tang and T. Yoshie, "Woodpile photonic crystal fabricated in GaAs by two-directional etching method," J. Vac. Sci. Technol. B **28**, 301–303 (2010).
25. A. Chutinan, S. John, and O. Toader, "Diffractionless flow of light in all-optical microchips," Phys. Rev. Lett. **90**, 123901 (2003).
26. A. Chutinan and S. John, "Light trapping and absorption optimization in certain thin-film photonic crystal architectures," Phys. Rev. B **78**, 023825 (2008).
27. S. John and R. Z. Wang, "Metallic photonic-band-gap filament architectures for optimized incandescent lighting," Phys. Rev. A **78**, 043809 (2008).

1. Introduction

The concept of photonic crystal (PhC) [1,2] has impacted number of fields in optics and beyond. Namely, the thresholdless lasing, bend-unrestricted waveguiding, control of black-body emission, all optical control of light propagation via optical nonlinearities were considered [3, 4]. Control of light absorption and emission by engineering photon density of states via periodic modifications of dielectric properties of material is at the core of a PhCs concept. Technical challenges are mounting for three-dimensional (3D) structuring of materials at sub-micrometer resolution [5]. Lithography based approach relies on 2D processing and usually requires multi-step procedures for fabrication of 3D micro-objects. It becomes increasingly difficult to fulfill high tolerances required for fabrication of PhCs operational at the visible spectral range [6, 7]. PhCs with full photonic bandgap (PBG) were demonstrated in near-IR at the telecommunication and longer wavelengths [8, 9]; recently lasing in 3D-PhC with a full PBG has been reported [10]. However, there are still no demonstrations of full PBG at the visible spectral range. In nature, opals and butterfly wings are probably the most known examples of larger area/volume structures where a 3D arrangement of materials with feature size of 100-200 nm delivers control over green-red visible spectral range. Yet this remains a challenging task for modern technology.

Earlier attempts to find scalable methods to fabricate 3D PhCs for near-IR and visible spectral range were based on complex multi-step approaches of laser photo-polymerization of a PhC template with subsequent inversion into a high refractive material [11, 12], a LIGA (X-ray

#141022 - $15.00 USD Received 12 Jan 2011; revised 1 Mar 2011; accepted 4 Mar 2011; published 14 Mar 2011

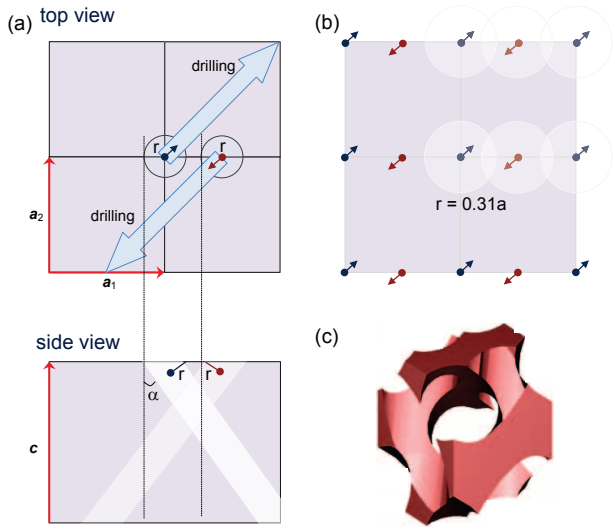

Fig. 1. (a) Slanted-pore $SP_2^{(1)}$ square structure [19]; ends of the arrows are on the depth c from surface. For the full photonic bandgap at 633 nm in TiO_2-rutile: $a = 260$ nm, $c = 1.4a = 363$ nm, $r = 0.31a = 80.6$ nm. (b) The "drilling map" on the (001)-plane of rutile with the angle to normal $\alpha = \arctan(a\sqrt{2}/c) = 45.3^\circ$. The circles mark diameters of the holes. (c) The unit cell.

Lithographic Galvanoformung and Abformung) based processing of thick PMMA films [13], and a combined photo-electrochemical etching of silicon with a direct write using a focused ion beam (FIB) [14]. Recently, a titania woodpile structure was fabricated with cell dimensions approaching those required for opening a complete photonic bandgap (PBG) at visible wavelengths (namely, a period of 250 nm with 70-nm-wide titania rods) using layer-by-layer fabrication with electron beam lithography (EBL), deposition, and plasma etching [15]. The template - inversion route is challenging due to severe constrains on mechanical strength of the structure [16] to maintain its integrity over several thermal and wet-bath chemical processing steps [17]. Even though single 3D features of few-tens-of-nm can be polymerized by femtosecond (fs)-laser direct write [18], PhC templates with periods ~ 0.3 μm are still challenging to obtain with photopolymer volume fraction of ~ 0.3 required for a complete PBG after double inversion; it is noteworthy that use of critical point dryer after a wet-bath development allows recovery of 3D templates with ~ 1.5 times smaller feature sizes. As for the standard LIGA and FIB approaches for material structuring with the required 100-200 nm resolution, it is at the limit of the current state-of-the-art. Higher resolution tools of material structuring with high efficiency are required to find new methods for reliable fabrication of 3D photonic structures at the visible spectral range of 0.4-0.8 μm wavelengths.

Here, we demonstrate a 3D ion beam lithography (IBL) approach in fabrication of a 3D PhC slanted-pore SP_2 structure [19], which has a wide and robust PBG, by a simple two-step direct write processing of rutile crystalline TiO_2. Geometry of the unit cell is chosen for the PBG at visible wavelengths. The fabrication technique does not require time and material consuming steps of resist and mask coatings with subsequent wet or dry processing. The direct patterning approach by Ga-ions is used to sculpture 3D PhC out of the crystal with resolution of tens-of-nanometers. Capability of of direct write at arbitrary angle in 3D mode is a distinctive feature of 3D-IBL. It is shown that, by using XeF_2 gas, enhancement of titania rutile etching

#141022 - $15.00 USD Received 12 Jan 2011; revised 1 Mar 2011; accepted 4 Mar 2011; published 14 Mar 2011

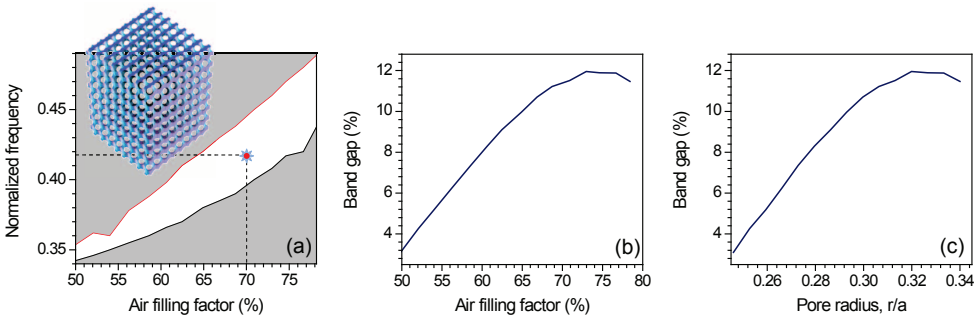

Fig. 2. (a) Photonic bands (grey) and gap (white) in terms of the normalized frequency, $\omega_n \equiv \omega a/(2\pi c)$. The marker representing parameters of the designed structure. Inset shows the slanted pore $SP_2^{(1)}$ PhC. (b) The width of the bandgap, $\Delta\omega/\omega$ (%), vs the air filling factor of the $SP_2^{(1)}$ structure for the dielectric constant of $\varepsilon = 7.4$ (TiO_2-rutile). (c) Width of PBG vs the pore radius normalized to the period a.

up to 5 times is achieved and is beneficial for high-aspect formation of pores. We discuss how the demonstrated high-aspect-ratio pore patterning in titania can be further improved by introducing trepanning and a concentric out-wards scanning of strongly focused ion beam during milling together with optimization of the dose and chemical enhancement. Hence, making the fabrication of PhC with full PBG at the visible spectral range feasible.

2. Design

The slanted-pore PhC structure [19] is chosen for its simplicity and its wide and robust photonic bandgap. The square $SP_2^{(1)} \equiv S/[1,1] \otimes [-1,-1]^{(0.5,0)}$ design [19] is shown in Fig. 1, where according to the nomenclature the drilling directions are opposite and shifted along vector $\mathbf{a}_1$ by a half of the period a, hence, $\ldots^{(0.5,0)}$. Over the period c in axial direction the pores travel sideways by one lateral period a; hence, the $[1,1] \otimes [-1,-1]$ notation for two opposite drilling directions.

The sample of TiO_2-rutile used in this study has a refractive index $n \simeq 2.7$ (the dielectric constant $\varepsilon_{TiO2} \equiv ((2n_o + n_e)/3)^2 = ((2 \times 2.621 + 2.919)/3)^2 \simeq 2.72^2 = 7.4$ at 579.1 nm) through the visible-to-IR spectral range with fundamental absorption edge at $E_g = 3.127$ eV ($\lambda_{[\mu m]} = 1.23976/E_g[\text{eV}] = 0.396\ \mu$m) [20].

The dependence of PBG and its width on the air filling factor and pore radius are calculated for the lossless $\varepsilon = 7.4$ material (Fig. 2). The plots are obtained using plane wave expansion technique (PWE). In this method the periodic refractive index is decomposed into its Fourier components and the Floquet Bloch modes are projected onto truncated plane wave basis, thus mapping the infinite dimensional Maxwell's equation for the band structure into a finite linear eigenvalue problem. The matrix equation is then solved numerically to yield the eigenvalues and eigenfunction solutions. In order to obtain the optimum design parameters, simulations were repeated for different pore radii or equivalently volume filling factors. The square lattice period, a, is related to the normalized frequency, $\omega_n \equiv \omega a/(2\pi c)$, which corresponds to the middle PBG position of $\omega_n \sim 0.41$ (marker in Fig. 2(a)) as $a = \omega_n \times \lambda_0$, here λ_0 is the vacuum wavelength. For the full photonic bandgap at the red wavelength of He-Ne laser $\lambda_0 = 633$ nm in TiO_2 the lateral period is $a \simeq 260$ nm and the axial period $c = 1.4a \simeq 363$ nm. The radius of the pore $r = 0.31a = 80.6$ nm for the PBG of $\sim 11.5\%$ [19]. This choice of parameters is robust in terms of slight deviations of the holes' radius and volume fraction (see, (b,c)). Removal of up to 70% of sample's volume is experimentally challenging; in case of a 1D PhC with refractive

#141022 - $15.00 USD Received 12 Jan 2011; revised 1 Mar 2011; accepted 4 Mar 2011; published 14 Mar 2011

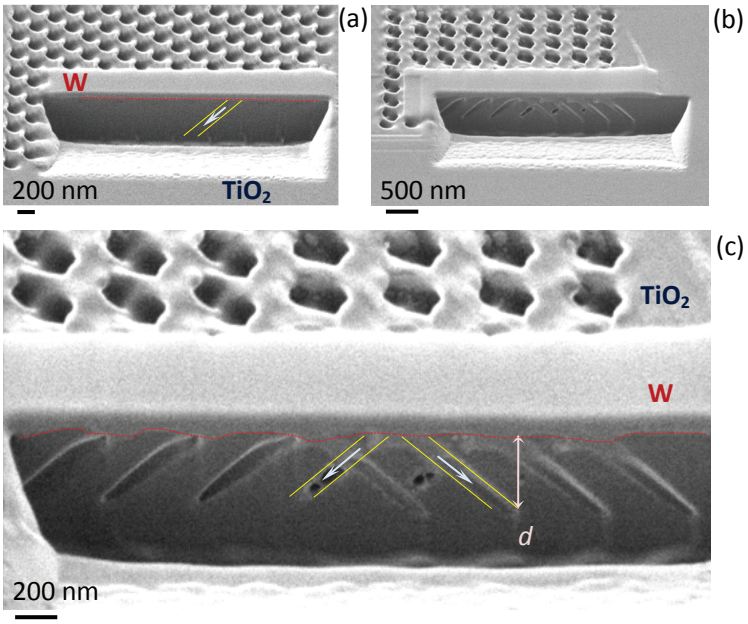

Fig. 3. Scanning ion microscopy images of the FIB cross section of a PhC structure after one (a) and two (b) directional pore recording; (c) is a closeup view of (b). Sample is at a $\pi/4$ tilt angle; designed pore radius $r = 40$ nm (the actual radius ~ 50 nm). The arrows depict direction of FIB processing, dashed-lines in (a) and (c) demarcate the TiO_2-W boundary, and d is the depth of the structure. Note, the cross section in (a) is not centered at the pores; partial filling of pores by W is observed close to the surface (c).

index n of solid part in air, the optimum solid volume fraction to create the largest PBG is $(1/2n)$.

3. Samples and methods

The samples of TiO_2-rutile (Shinkosha, Ltd.) were used for the 3D patterning by Ga-ions (Raith ionLiNE). Chemical enhancement of titania removal is tested using a XeF_2 gas. For cross sectioning of 3D patterns of slanted pores, a standard over-top deposition of tungsten from a $W(CO)_6$ precursor was implemented before ion slicing. Samples were directly imaged using secondary electron emission from surface scanned by ion beam, the scanning ion microscopy (SIM), at low current to avoid surface removal.

Transmission spectra for the finite size PhCs were simulated using finite difference time domain (FDTD) program *Lumerical*. The model of the structure was constructed by stacking PhC unit cells as in Fig. 1(c) in the z-direction up to the desired slab height. The material was modeled by using the experimental dielectric functions available in literature [21]. The crystal was illuminated by a plane-wave source delimited by periodic boundary conditions in the normal incidence case, and Bloch boundary conditions were employed for determining the angular transmission spectra while tilting the source incidence angle in the x-direction. As the Bloch boundary conditions are tuned for a constant value of the transverse k-vector k_x this, for broadband time-domain simulations, involves a wavelength dependency of the incidence angle $\theta = \arcsin(\lambda k_x/2\pi n)$. Thus, simulations are performed for constant k_x and the results are interpolated for constant θ. Simulation time is around 15 minutes for a 5 ps broadband pulse

#141022 - $15.00 USD Received 12 Jan 2011; revised 1 Mar 2011; accepted 4 Mar 2011; published 14 Mar 2011

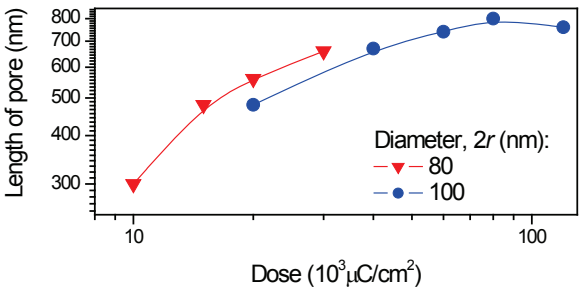

Fig. 4. Length of channel at different diameters, $2r$, measured by cross sectioning and imaging with the scanning ion microscopy; lines are eye guides.

propagation time.

4. Results and discussion

4.1. 3D sculpturing of rutile by direct write

Ga-ion patterning by IBL is used for fabrication of 3D slanted-pore PhC structure consisting of holes drilled into TiO_2 substrate at angle $\alpha \equiv \arctan(a\sqrt{2}/c) \simeq 45.3^\circ$ to the surface normal by a circular scan of the ion beam. The resolution of ion-beam patterning was approximately 10 nm entitling to fabricate 3D structures. The resulting structure is a realization of $SP_2^{(1)}$ shown in Fig. 1. Parameters of the structure are chosen for the PBG to be at the 633 nm wavelength which is longer than the fundamental absorption of rutile at approximately ~ 396 nm. Visualization of the unit cell of the 3D PhC structure is shown in the inset of Fig. 2(a).

The $SP_2^{(1)}$ structure was directly recorded in TiO_2-rutile with (001) face-plane (see, Fig. 1) with the parameters as close as possible to those required for an opening of the full photonic bandgap: $a = 260$ nm, $c = 363$ nm, $r = 80$ nm (radius). The angle to normal of each pore is $\alpha = 45.3^\circ$.

Figure 3 shows SIM images of the cross-sectioned structure revealing the slanted pore pattern. The period of the structure is $a = 260$ nm with pore radius of 40 nm, which is smaller than $r = 0.31a = 80.6$ nm required for the PBG opening. When the edges of the neighboring pores begin to overlap at larger radius of the pores, a strong etching of the previously drilled pore's edge occurs; up to three times faster ion milling of the edge takes place as compared with drilling of far-separated pores on in the bulk. Hence, overlapping of pores was avoided in the first experiments and the designed pore radii of 40 and 50 nm were used instead (note, the radii of the actual fabricated pores was up to 20% larger as compared with the design values). A strategy of fabricating overlapping pores of the required radius will be outlined below.

The depth of the fabricated structure, d, is directly measured at the $\pi/4$-tilted view. Then the actual length of the pore is $l = 2d$ accounting for an additional $\pi/4$ tilt in the plane of cross section. The pores formed at the first tilt were closely following the designed pattern (Fig. 3), however, for the second tilted drilling the proximity of already formed pores caused charging and gradual misalignment of the pattern as recording progressed (see slight change of the pattern recognizable in panels (b,c)). Fortunately, the same designed depth of the pores was achieved. In this fabrication no anti-charging measures were taken.

Figure 4 shows that the aspect ratio $f_{ar} = l/(2r)$ reaches value of $f_{ar} \simeq 8$ for the 100-nm-diameter pores. At this value the the length of the channel was already saturated. To make channels longer chemical enhancement by XeF_2 gas is a common practice, e.g., in an etching resistant sapphire the enhancement of ion milling up to 2 times has been reported [22]. To

#141022 - $15.00 USD Received 12 Jan 2011; revised 1 Mar 2011; accepted 4 Mar 2011; published 14 Mar 2011

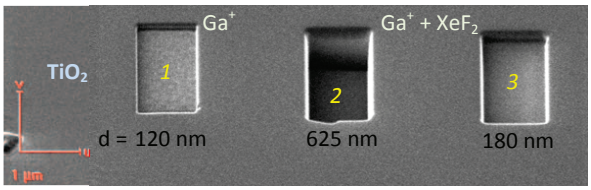

Fig. 5. Chemical enhancement of ion processing of titania. Scanning ion microscopy images of the TiO_2 surface processed without (region *(1)*; as in Fig. 3) and with (region *(2,3)*) chemical enhancement provided by the XeF_2 gas. The region *(3)* corresponds to a ~ 1 mm nozzle (of XeF_2) distance to the substrate as in the actual tilted drilling shown in Fig. 3.

test a possibility and quantify etching speed changes due to the chemical enhancement, a large area pit fabrication was performed by Ga-ion beam on titania. Figure 5 shows the actual 5.2 times enhancement observed due to the gas addition (the depth of the region *(2)* vs *(1)*). The region *(3)* corresponds to the nozzle-to-substrate distance as in the actual fabrication of patterns shown in Fig. 3 with enhancement of 1.5 times due to larger separation between the nozzle and a tilted sample. Hence, for fabrication of deeper pores the chemical enhancement can be used. An optimization of the pore formation protocol under conditions of chemical enhancement, however, needs to be developed since the enhancement affects the pore's diameter and speed of the edge milling in a nonlinear fashion, i.e., the low intensity wings of the ion beam causes strong etching and loss of a pointing precision of milling, while, at the center of the beam, there is saturation of etching speed.

Figure 6 shows simulated transmission spectra, T, for the $SP_2^{(1)}$ PhC with pores of different diameters and lengths. The structure with $r = 50$ nm (as in our experiments) and with the pore length of $l = 1.5$ μm shows a strong 14.7 dB rejection at the normal incidence. This particular length is chosen as a practically achievable one. Indeed, at the already obtained aspect ratio, $f_{ar} = 8$, and chemical enhancement of 1.5 (see, region *(3)* vs *(1)* in Fig. 5) for the required diameter $2r = 160$ nm, one would obtain the length estimate $l = 1.5 \times 2r \times f_{ar} \simeq 1.9$ μm. The stop band is centered at the edge of optical spectral range with center wavelength of 800 nm (Fig. 6(a)). For a shorter pore length (see, (b)) the stop gap is less prominent and disappears

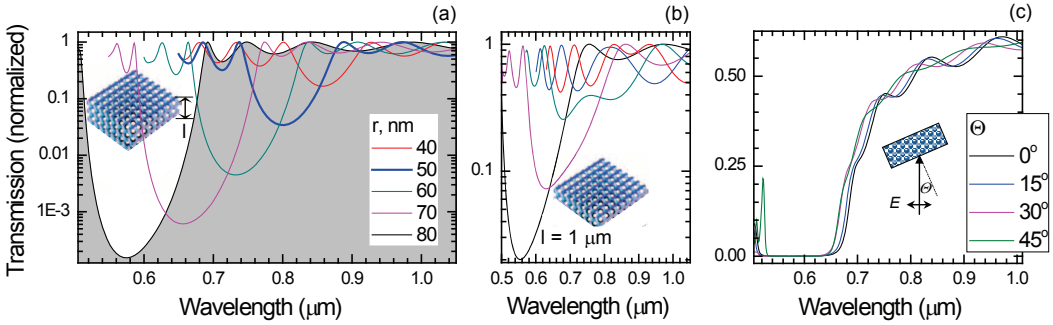

Fig. 6. FDTD simulated transmission spectra at normal incidence for different pore radii, r, of slanted pore $SP_2^{(1)}$ PhC with the pore length: $l = 1.5$ μm (a) and 1 μm (b). The insets shows the $SP_2^{(1)}$ structure of the volume fraction required for the full photonic bandgap at $r = 80$ nm. (c) Angular transmission spectra for the $r = 80$ nm and $l = 1.5$ μm-thick structure. Angle of incidence, Θ, polarization is linear.

#141022 - $15.00 USD Received 12 Jan 2011; revised 1 Mar 2011; accepted 4 Mar 2011; published 14 Mar 2011

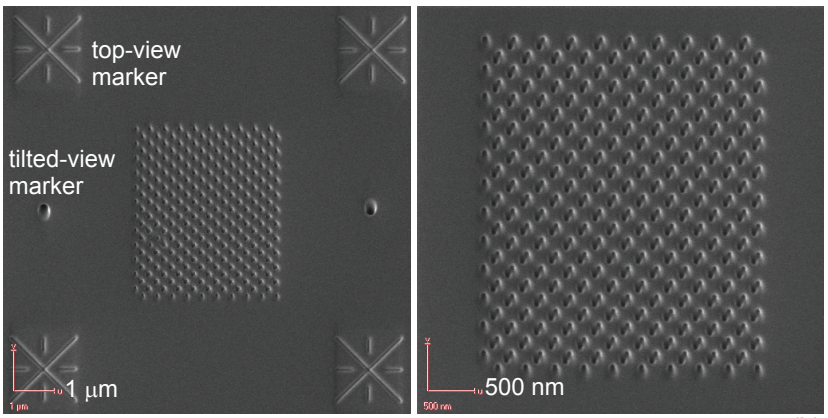

Fig. 7. Scanning ion microscopy images of a $SP_2^{(1)}$ PhC pattern using an anti-charging coating ($\sim$ 10 nm of Pt). The top- (at corners) and tilted-view (two at the sides) markers facilitate precise toggling between $+\pi/4$ (the left marker) and $-\pi/4$ (right) to the normal in a multi-step hole drilling using trepanning and concentric scans.

more rapidly as volume fraction of air decreases.

4.2. Tolerances of structure parameters

Up to now, the proof-of-the-principle demonstration of the 3D PBG formation is achieved in Si [23] and GaAs [24] at 1.5 μm wavelength. The *aspect ratio*, $f_{ar} = \frac{length}{diameter}$, of the slanted pores was $\simeq 10$ for the omnidirectional photonic band to be experimentally validated [23]. For the our $SP_2^{(1)}$ structure with diameter $2r = 160$ nm and $c = 363$ nm, the PBG at 633 nm assuming the same $f_{ar} = 10$ would require just three axial periods of the structure: $f_{ar} \times 2r/(c \times \cos(\alpha)^{-1}) \simeq 3.1$.

Numerical simulations of transmission, T, spectra (Fig. 6) show that for a slightly smaller aspect ratio of pores (5–6) the stop gap disappears. The angular dependence of the PBG in a $l = 1.5$ μm-thick slab of the unit cell and volume fraction required for the complete PBG (Fig. 6(c)) shows the band narrowing within an envelope of PBG rather than a strong spectral shift as would be expected for incomplete PBG. PhC structures of larger thickness have to be fabricated for the actual optical characterization.

The SP_2 structure gives more flexibility to create a larger PBG since the air rods can actually overlap, whereas the TiO_2 rods of the woodpile [15] can at most touch but cannot overlap. Also the quality of crystalline TiO_2 is likely better and the refractive index is higher as compared with sputtered/evaporated titania films $n = 2.3$ [15].

4.3. Scaling prospects for large area nano-patterning

In this study, we used the maximum radius of $r = 50$ nm when the pores are at the limit of overlap. Since drilling of the required diameter holes in a single step causes strong pattern alterations due to excessive charging and preferential pore's edge milling, a multi-step drilling of pores with a gradually increasing diameter should be exercised for the functional patterns. Also, a trepanning with concentric out-wards scanning of a strongly focused ion beam during milling together with optimization of the dose, however, it requires the outmost stability of sample positioning and movement control. An exact protocol for removal of up to 70% of

#141022 - $15.00 USD Received 12 Jan 2011; revised 1 Mar 2011; accepted 4 Mar 2011; published 14 Mar 2011

titania in a well controlled way is yet to be established. However, it is obvious that pores should be made in several consequential drilling steps.

To facilitate a repeated drilling of pores, toggling of sample is required. Markers at the top- and tilted-view are used to optimize sample positioning (Fig. 7). Such markers allow to toggle and set sample with precision ± 10 nm. The size of a structure required for the optical characterization is 60×60 holes (or $\sim 15 \times 15\ \mu\text{m}^2$) area drilled to a $\sim 2\ \mu$m depth. The time required for a single pore milling is few seconds, hence, time required for a large area sample for optical characterization would take several hours. For the larger pore diameters the aspect ratio is expected to increase (see, Fig. 4) even without chemical enhancement. It is noteworthy, that high-vacuum conditions of $\sim 10^{-7}$ bar were essential to obtain deep pores without apparent material redeposition.

Metal or anti-charging coating must be used to fabricate large areas with tens-of-μm in cross section for optical characterization. No changes of a pattern geometry were observed during ion fabrication over a 10-nm-platinum coated substrate as illustrated on a smaller area in Fig. 7.

The achieved aspect ratio of ~ 10 is already enough for the proof-of-the-principle demonstration and improves upon earlier demonstration of Si milling by FIB [14]. Moreover, the SP_3 structure used in previous experiments [14] is more complex to fabricate and has narrower bandgap as compared with the SP_2 structure demonstrated here by a two-step milling approach.

5. Conclusions

Ion beam direct writing is proposed as a tool to form PhC structures with the feature sizes required for functionality at the visible spectral range. The maskless direct write approach using IBL enters a promising parameter space of 100 nm feature size required for precise control of functionality of PhC structures at visible wavelengths. Numerical modeling of the fabrication tolerances in terms of pore radius and structure thickness demonstrates potential of high-resolution 3D-IBL in the field of photonic applications. Implementing anti-charging coating and fabricating pores with increasing diameter in several runs is expected to deliver required quality of the 3D PhC needed for demonstration of full PBG at the visible wavelengths. PhCs have important practical applications in confining light on an optical micro-chip for all-optical information processing, in trapping and absorbing light in thin films for efficient solar energy harvesting, and novel light emitters, to mention a few [25–27].

Acknowledgments

This work was supported in part by Swinburne University of Technology startup funding and the Natural Sciences and Engineering Research Council of Canada. S. Juodkazis is grateful to Austrade for a research visit support to Raith, Ltd.

#141022 - $15.00 USD Received 12 Jan 2011; revised 1 Mar 2011; accepted 4 Mar 2011; published 14 Mar 2011